State-Space Modeling and Small-Signal Stability Analysis of an Independent Microgrid with Multiple Distributed Generation Resources

Mohammad Yousefzadeh * iD , Hamid Reza Najafi * iD , Hussein Eliasi * iD

* Faculty of Electrical and Computer Engineering, University of Birjand, Birjand, Iran

(mm.yousefzadeh68@gmail.com, h.r.najafi@birjand.ac.ir, h_eliasi@birjand.ac.ir)

‡ Corresponding Author; Mohammad Yousefzadeh, Postal address, Tel: +98 935 695 5194,

Fax: +90 312 123 4567, corresponding@affl.edu

Abstract- The integration of distributed generation (DG) resources, energy storage systems (ESS), and local electric loads within a specific region has given rise to the concept of microgrid as a significant aspect of smart grids. This research addresses the small signal stability analysis of a an independent microgrid with multiple DG resources while considering the modeling of each DG resource through eigenvalue analysis and frequency response analysis. The microgrid comprises a squirrel cage induction generator-wind turbine (SCIG-WT) as DG1, a diesel synchronous generator (DSG) set equipped with governor and excitation controllers as DG2, an inverter-based battery energy storage system (BESS), and a set of lines and loads. At first, each resource is individually modeled in its respective local state-space reference frame. These individual models are then combined in a global reference frame. The microgrid's global model is linearized around a specific operating point, resulting in the derivation of the system state matrix, from which the eigenvalues of the microgrid are obtained. The impact of varying system parameters and different operational conditions on the stability margin and microgrid dynamics is assessed by examining changes in eigenvalue locations and conducting sensitivity analysis. Finally, transfer functions of BESS controllers are determined, allowing for a frequency response analysis concerning the controller coefficients.

Keywords: Microgrid, State-Space Modeling, Small-Signal Stability, Energy Storage System (ESS), Eigenvalue Analysis, Frequency Response Analysis.

1. Introduction

Smart grid technology has received plentiful attention in past years to develop the traditional power distribution network and to enable the integration of DG units to satisfy load demand growth and to enhance network performance [1]. The continued expansion of DG resources in electrical energy generation, driven by their technical, economic, and environmental advantages, represents an ongoing trend. The capability of installing DG resources close to the sensitive loads which need reliability and high-power quality has been resulted in emerging the concept of microgrids in power systems. A microgrid is a hybrid electric network comprising DGs, ESSs and local loads for supplying power to specific areas or remote locations, with a primary function of guaranteeing the system's stability on the occurrence of different faults [2]. Microgrids can function both connected to a larger continuous grid for power exchange and independently from it. Fundamentally, one of the primary reasons for introducing the microgrid concept is increasing the renewable energy resources integration into power grids [3].

The stability of microgrids is a fundamental principle in dynamic studies and serves as a central focus in their operation. It plays a pivotal role in the energy management and planning of microgrids. The analysis of stability is a critical component in system security analysis, and ensuring the safe and secure operation of microgrids requires precise

assessments of stability. Key elements in the stability analysis of microgrids include considerations of voltage and frequency stability.

In microgrids featuring a substantial number of voltage source converters (VSC) as power electronic interfaces for connecting distributed energy resources to the main grid, the discussions on stability are significantly contingent upon the control strategies employed for VSCs. However, it is crucial to acknowledge that other factors, such as energy storage, existing distributed resources, protection mechanisms, compensation techniques, and more, also have a considerable impact on the system's stability [4]. [4] and [5] are valuable resources for delving into various aspects of stability in microgrids. These comprehensively discuss the classification of stability problems, the factors responsible for each type of instability, and a wide range of solutions for addressing them.

Among the various types of stability, small-signal stability stands out as a critical concern for ensuring the reliable operation of microgrid [6]. This concern becomes even more pronounced in microgrids, particularly when operating in islanded mode with limited inertia. Low-inertia networks are susceptible to sudden disturbances and can become unstable due to common frequency deviations [7]. To enhance stability in such low-inertia networks, it is crucial to increase the amount of stored energy that can be easily accessed within the network. One effective approach to achieving this is the creation of virtual inertia through the utilization of the ESS.

Various dynamic models have been proposed for the investigation of small-signal stability in microgrids, covering both conventional and electromechanical sources [8-15], such as the impedance method and Lyapunov's direct method [16]. In [17], a dynamic model of an inverter is examined for small-signal stability studies. A systematic approach to the modelling of microgrids with droop controlled inverters for modal analysis was first introduced in [18]. [19] introduces a comprehensive small-signal model of a microgrid, which includes a synchronous generator equipped with an excitation and governor system, inverter-based sources, and a power network. Throughout this research, the dynamic characteristics of the system in standalone operation were thoroughly analysed. However, it's important to note that this model does not incorporate a wind turbine, which serves as a significant DG source. Dynamic modelling and small-signal stability analysis of microgrids involving inverter-based DGs with multiple converters are addressed in [20] and [21], respectively.

In the field of small-signal stability analysis, research articles commonly utilize techniques such as eigenvalue analysis and root locus analysis. Small-signal stability analysis assumes that disturbances are sufficiently small, facilitating the linearization of system equations around the initial operating point.

The present research introduces a dynamic model for the analysis of small-signal stability in an independent microgrid within a d-q rotating reference frame. This model considers the dynamic representation of each DG source within the microgrid. The model comprises several key components: (1) Rotating DG units within the microgrid, including SCIG-WT and synchronous DGS. (2) BESS with power electronic interfaces, (3) The power network, which encompasses transmission lines, loads, and series and parallel equipment, is mathematically formulated and systematically analysed. Initially, each source is individually modelled within its local state-space representation. These individual models are then integrated into the global reference frame. Subsequently, the impact of changing system parameters and various operating conditions on the microgrid's dynamics and stability margins is examined. This assessment involves the observation of changes in eigenvalues and the conduct of sensitivity analysis. Moreover, the aim is to determine the optimal range and investigate the influence of each controller coefficient on the frequency response of the transfer functions related to active and reactive power of the BESS controller. To facilitate this, the bode diagrams are created for each coefficient's variation, allowing the sensitivity of the system to be investigated with respect to changes in each of the coefficients. Presentation of a systematic approach for dynamic modelling of microgrid with multiple DG resources and frequency analysis of the BESS controller consider as the novelty of the research. The dynamic model obtained and the sensitivity analysis of eigenvalues can be used for the following purposes:

☐ Investigating the dynamics of the microgrid.

☐ Identifying and determining the secure operating points of DG units.

☐ Designing microgrid controllers, including the governor and exciter systems for diesel generator units, and active and reactive power controllers for DG resources with power electronic interfaces.

☐ Assisting in the development of suitable operational strategies to adapt to different combinations of DG units and operating conditions.

☐ Optimizing the control parameters of DG units based on power electronic converters to achieve the benefits of rapid response in improving voltage quality, frequency control, and stability preservation during transitions from one operating state to another.

☐ Optimizing various configurations of DG units to increase stability margins.

2. State-Space Modeling of Independent Microgrid with Multiple DG Sources

Figure 1 illustrates the structure of a low-voltage independent microgrid featuring multiple DG sources, designed in order to dynamic performance study. This microgrid comprises three radial feeders, numerous local loads, SCIG-WT as the DG1 source, a synchronous diesel generator set (DGS) equipped with governor and excitation controllers as the DG2 source, Inverter-based BESS, along with current and active/reactive power controllers. Distribution feeders and constant loads in each phase are represented as RL series consisting of a resistor (R) and an inductor (L), while the existing fixed capacitor bank is

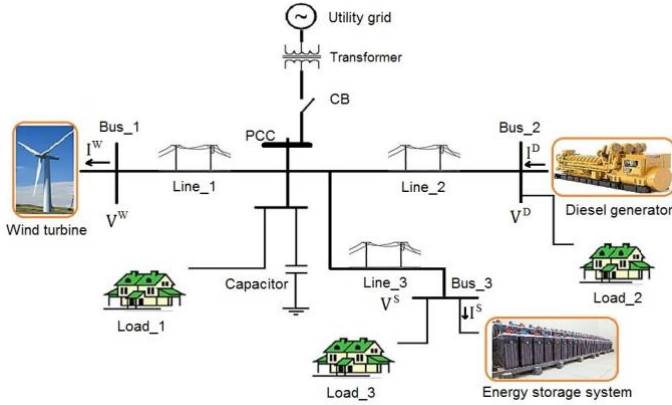modelled as a parallel capacitor (Cp) at the point of common coupling (PCC) bus.

Fig. 1. The microgrid under study for small-signal stability analysis.

To analyze the dynamic behavior of the microgrid, a general form of the state-space model for the microgrid is formulated as follows:

$$\Delta \dot{x} = A\Delta x + B\Delta u \tag{1}$$

This model is derived from the ordinary differential equations governing four main subsystems: the SCIG-WT, DSG with governor and excitation controllers, the BESS, and the power network, which encompasses lines, loads, and a fixed capacitor bank.

The modeling approach presented for the microgrid in Figure 1 is structured as follows: Initially, the microgrid system is divided into four main subsystems. To create the state-space model for the microgrid, the state-space model of each subsystem is first developed separately in its own local reference frame. Subsequently, a common reference frame is selected as the global reference frame for the microgrid system, and all the subsystems are then transformed into the global reference frame using the technique described in (2). Following linearization around an operating point, the general form (1) is derived.

$$\begin{bmatrix} \Delta f_q^g \\ \Delta f_d^g \end{bmatrix} = \begin{bmatrix} \cos\delta_n^o & \sin\delta_n^o \\ -\sin\delta_n^o & \cos\delta_n^o \end{bmatrix} \begin{bmatrix} \Delta f_q^n \\ \Delta f_d^n \end{bmatrix} + \begin{bmatrix} f_d^{go} \\ -f_q^{go} \end{bmatrix} \Delta\delta_n \tag{2}$$

$$T_n = \begin{bmatrix} \cos\delta_n & \sin\delta_n \\ -\sin\delta_n & \cos\delta_n \end{bmatrix}$$

In equation (2), the vectors $f^g = \begin{bmatrix} f_q^g & f_d^g \end{bmatrix}^T$ and $f^n = \begin{bmatrix} f_q^n & f_d^n \end{bmatrix}^T$ represent the vector of variable components f in the global reference frame and the local reference frame of the nth subsystem, respectively. δ_n is the angle between the d-axis of the global reference frame and the d-axis of the local reference frame of the nth subsystem.

The superscript "o" denotes the value at the operating point, and the matrix T_n represents the transformation matrix.
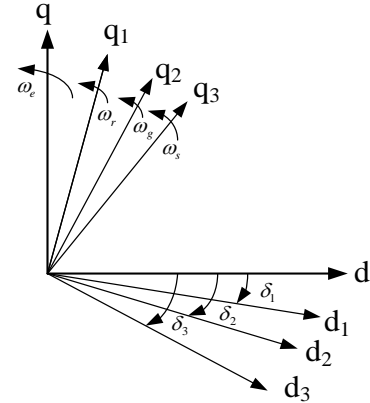

Fig. 2. Local and global rotating reference frames for the studied microgrid

As shown in Fig. 2, a global rotating reference frame with axes d and q is defined, and it rotates at an angular velocity ω_g. The axes d_1-q_1, d_2-q_2, and d_3-q_3 represent the local reference frames for SCIG-WT, DGS, and BESS, respectively. Each of these frames rotates at angular velocities ω_1, ω_2, and ω_3, respectively.

2.1. State-Space Dynamic Model of the SCIG-WT(DG1)

SCIG-WT comprises a wind turbine, the squirrel-cage induction generator and rotating shaft. The dynamic model of the DG1 can be divided into two parts: the electrical system and the mechanical system. The electrical system of the three-phase induction generator in its arbitrary reference frame d1-q1 is defined as follows:

$$V^W = EI^W + F\frac{d}{dt}(I^W) \tag{3}$$

$$V^W = \begin{bmatrix} V_{sq1} & V_{sd1} & V_{rq1} & V_{rd1} \end{bmatrix}^T$$

$$I^W = \begin{bmatrix} i_{sq1} & i_{sd1} & i_{rq1} & i_{rd1} \end{bmatrix}^T$$

In this equation, V^W and I^W represent the vector of generator terminal voltages and the generator currents, respectively. The matrices E and F are obtained from [22]. The mechanical model of the rotor of the induction generator is described as follows:

$$\frac{d\omega_r}{\omega_b dt} = \frac{1}{2H_i}(T_e - T_m) \tag{4}$$

where ω_r and ω_b represent the rotor electrical angular velocity and the base electrical angular velocity, respectively. H_i is the total rotor inertia constant. T_m is the mechanical

torque and T_e is the electromagnetic torque. The electromagnetic torque (T_e) is calculated as:

$$T_e = X_m \left(i_{rd1} i_{sq1} - i_{rq1} i_{sd1} \right) \tag{5}$$

where X_m is the mutual reactance between the stator and rotor windings.

Because the electromagnetic torque equation contains two variables, linearization is achieved using the Taylor expansion method with a constant value. The aerodynamic characteristics related to the wind turbine are expressed as follows:

$$\begin{cases} \lambda = R_c \dfrac{\omega_t}{V_{wind}} \\ T_w = \dfrac{1}{2} \rho \pi C_T(\lambda,\beta) V_{wind}^2 R_c^3 \end{cases} \tag{6}$$

where λ is the tip-speed ratio, defined as the ratio of the speed of the tip of the aerodynamic rotor blade to the wind speed. R_c is the sweep area of turbine blades, ω_t is the angular speed of turbine rotation, V_{wind} is the wind speed, ρ is the air density, $C_T(\lambda,\beta)$ is the torque coefficient. β is the blade pitch angle and T_w is the mechanical torque of wind turbine. The wind turbine is mechanically connected to the induction generator through a coaxial shaft. Due to its significant inertia, its mechanical characteristics can be approximated as that of a first-order time-delay system, as illustrated below:

$$\frac{dT_m}{dt} = \frac{1}{T_H} (T_w - T_m) \tag{7}$$

where T_H is the inertia time constant.

The state-space model of DG1 in the rotor rotating frame (d_1-q_1) is derived by combining the dynamic models of the electrical system (equation 3) and the mechanical system (equation 7). The resulting integrated model is subsequently converted into the global reference frame (d-q) employing the transformation matrix outlined in (2). The linearized state-space model in the global reference frame is expressed in the following form:

$$\Delta \dot{x}_W^g = A_W \Delta x_W^g + B_W^v \Delta v^W + B_W^u \Delta u^W \tag{8}$$

$$\Delta x_W^g = \begin{bmatrix} \Delta i_{sq1}^g & \Delta i_{sd1}^g & \Delta i_{rq1} & \Delta i_{rd1} & \Delta \omega_r & \Delta T \end{bmatrix}^T$$

$$\Delta v^W = \begin{bmatrix} \Delta V_{sq1}^g & \Delta V_{sd1}^g \end{bmatrix}^T$$

$$\Delta u^W = \begin{bmatrix} \Delta V_{rq1} & \Delta V_{rd1} & \Delta V_{wind} \end{bmatrix}^T$$

Δx_W^g is the state variable vector of DG1. Δv^W and Δu^W are the linearized stator voltage vector and the input control signals vector of DG1, respectively.

2.2. State-Space Dynamic Model of Diesel Synchronous Generator (DG2)

DG2 comprises a diesel engine and a three-phase synchronous generator featuring excitation and governor control systems. The dynamic model of the synchronous generator is divided into two parts: the electrical system and the mechanical system. The ordinary differential equations (ODEs) that represent the electrical dynamics of the synchronous generator in the rotor rotating reference frame d2-q2 are defined as follows:

$$V^D = G I^D + H \frac{d}{dt} (I^D) \tag{9}$$

where

$$V^D = \begin{bmatrix} V_{sq2} & V_{sd2} & V_{k1q2} & V_{k2q2} & V_{kd2} & V_{fd2} \end{bmatrix}^T$$

$$I^D = \begin{bmatrix} i_{sq2} & i_{sd2} & i_{k1q2} & i_{k2q2} & i_{kd2} & i_{fd2} \end{bmatrix}^T$$

are the voltage and current vectors of stator windings $(sq2,sd2)$. $k1q2$, $k2q2$, and $kd2$ represent the damper winding elements. $fd2$ is field winding. G and H matrices are determined based on the [22].

The mechanical system of the DG2 rotor is approximated as a solid rotating mass, and the dynamic model of this mass in rotation is defined as follows:

$$\frac{2H_s}{\omega_b} \frac{d\omega_r}{dt} + \frac{D_a}{\omega_b} \frac{d\delta_2}{dt} = T_M - T_{es} \tag{10}$$

where H_s and inertia and damping rotor'sare D_a constants respectively. ω_1 represents the electrical angular velocity of the rotor. T_M is the mechanical torque. T_{es} is the electromagnetic torque generated at air gap and can be determined as follows:

$$T_{es} = \frac{3}{2\omega_r} \left(v_{q2} i_{q2} + v_{d2} i_{d2} \right) = X_{md} i_{q2} \left(i_{fd2} + i_{kd2} - i_{d2} \right)$$

$$- X_{mq} i_{d2} \left(i_{k1q2} + i_{k2q2} - i_{q2} \right) \tag{11}$$

where, X_{md2} and X_{mq2} are magnetizing reactance.

The state-space model of DG2 in the global reference frame of the microgrid, is represented in the following standard form:

$$\Delta \dot{x}_D^g = A_D \Delta x_D^g + B_D^v \Delta v^D + B_D^u \Delta u^D \tag{12}$$

$$\Delta x_D^g = \begin{bmatrix} \Delta i_{sq2}^g & \Delta i_{sd2}^g & \Delta i_{k1q2} & \Delta i_{k2q2} & \Delta i_{kd2} & \Delta i_{fd2} & \Delta \delta_2 & \Delta \delta_2 \end{bmatrix}^T$$

$$\Delta v^D = \begin{bmatrix} \Delta V_{sq2}^g & \Delta V_{sd2}^g \end{bmatrix}^T$$

$$\Delta u^D = \begin{bmatrix} \Delta V_{fd2} & \Delta T_m \end{bmatrix}^T$$

where, Δx_D^g represents the state variables vector of DG2. The vector Δv^D represents the linearized stator voltage in the global reference frame of the microgrid, and Δu^D is the vector of control signals input from the excitation and governor system.

2.3. State-Space Dynamic Model of the BESS

The BESS comprises a battery bank, power electronic converter, associated control systems, and filters. Figure 3 presents a schematic depiction of the storage unit within the microgrid. To model the energy storage system, two distinct subsystems are employed: the power circuit and the control system.

2.3.1. Power Circuit Model of the BESS

In modeling an inverter-based energy source, it is assumed that the controllers maintain a stable DC link voltage. Consequently, the primary energy source has negligible influence on the steady-state model [23]. In the present study, the DC side is idealized as a constant voltage source, denoted as Vdc. On the AC side of the converter, each phase is represented as a series connection of elements R and L, symbolizing the series filter components and transformer. The dynamic model of the AC side power circuit, in the local frame d3-q3, is expressed as follows:

$$\frac{d}{dt} i_{d3}^S = -\frac{R_{Bf}}{L_{Bf}} i_{d3}^S + \omega_b i_{q3}^S + \frac{1}{L_{Bf}}\left(V_{d3}^S - V_{d3}^B\right)$$

$$\frac{d}{dt} i_{q3}^S = -\frac{R_{Bf}}{L_{Bf}} i_{q3}^S - \omega_b i_{d3}^S + \frac{1}{L_{Bf}}\left(V_{q3}^S - V_{q3}^B\right) \quad (13)$$

where, V_{d3}^B and V_{q3}^B are the voltage components of the converter, V_{d3}^S and V_{q3}^S are the components of AC bus voltages, and i_{d3}^S and i_{q3}^S are the converter current components in the d3-q3 local frame.

The final state-space model of the BEES power circuit, obtained by transforming it into the global reference frame of the microgrid using Equation (2) and linearizing it around a specific operating point, is expressed as follows:

$$\Delta \dot{x}_{Sp}^g = A_{Sp}^g \Delta x_{Sp}^g + B_{Sp}^v \Delta v^S + B_{Sp}^u \Delta u_s + B_{Sp}^\omega \Delta \omega_3 \quad (14)$$

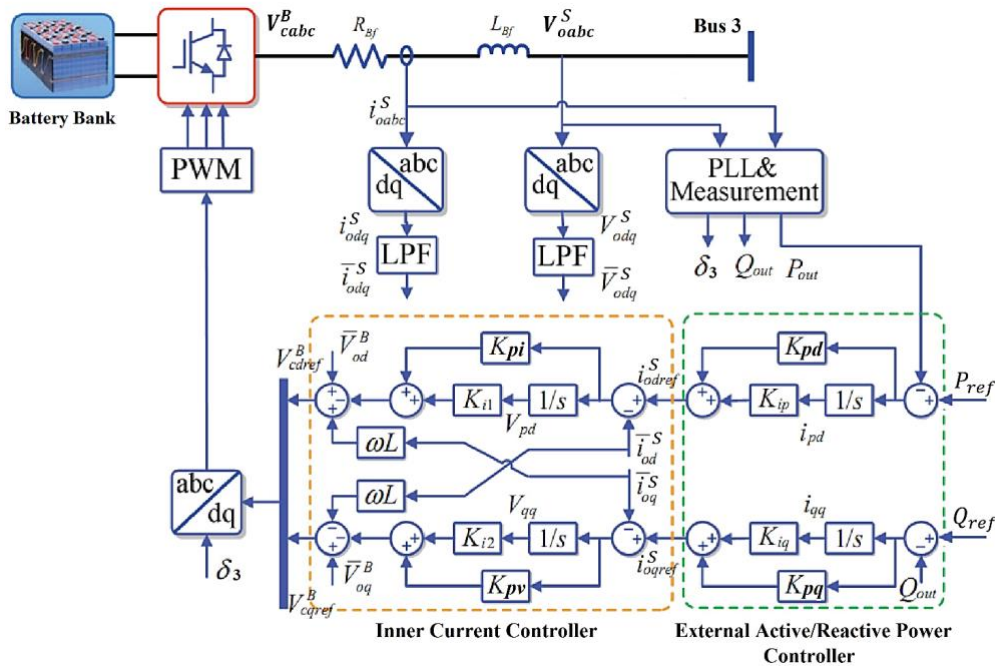$$\Delta x_{Sp}^g = \begin{bmatrix} \Delta i_{q3}^S & \Delta i_{d3}^S \end{bmatrix}^T$$

Fig. 3. Power circuit and control structure of BESS.

2.3.2. Energy Storage System Control

The active and reactive powers of the energy storage output are regulated by the instantaneous values of the AC side current components of the converter, namely, i_{d3}^S and i_{q3}^S, respectively. The control system comprises three controllers: two inner current loop controllers for managing the d and q components of the converter current, a voltage feedforward controller, and two outer control loops that generate reference values for the inner loops based on the desired active and reactive powers at the converter terminal.

The input signals to the current control block, i_{d3}^S and i_{q3}^S, undergo filtering through two low-pass filters (LPF). In practical application, these low-pass filters play a crucial role in eliminating noise and filtering out output harmonics. The inner current controller and the voltage feedforward controller produce reference voltages, V_{cdref}^B and V_{cqref}^B, for the converter. As illustrated in Figure 3, the current and power controllers are implemented using conventional PI controllers.

Referring to Fig. 3, the estimation of the phase angle of the bus voltage and the calculation of the instantaneous active and reactive powers for bus 3 involve the utilization of a phase-locked loop (PLL) block and a measurement block. The mathematical model of the PLL is presented as follows:

$$\Delta\dot{\omega}_3 = -K_{pll}\left[K_{pw}\Delta\omega_3 + K_{iw}\left(\Delta\delta_{3ref} - \Delta\delta_3\right)\right] \qquad (15)$$

where K_{pll} represents the bandwidth of the input signal to the main PLL block, and K_{pw} and K_{iw} are proportional and integral gains of the PI controller. The state-space representation of the linearized control system of BESS in the global reference frame of the microgrid will be as follows:

$$\Delta\dot{x}_{Sc}^g = A_{Sc}\Delta x_{Sc}^g + B_S^p\Delta x_{Sp}^g + B_{Sc}^v\Delta v^{Sc} + B_{Sc}^u\Delta u_{Sc} \qquad (16)$$

where

$$\Delta x_{Sc}^g = \begin{bmatrix} \Delta\bar{V}_{q3}^S & \Delta\bar{V}_{d3}^S & \Delta\bar{V}_{q3}^B & \Delta\bar{V}_{d3}^B & \Delta i_{qq} & \Delta i_{pd} & \Delta\bar{i}_{q3}^S & \Delta\bar{i}_{d3}^S & \Delta V_{qq} & \Delta V_{pd} & \Delta\omega_3 \end{bmatrix}^T$$

$$\Delta v^{Sc} = \begin{bmatrix} \Delta V_{q3}^S & \Delta V_{d3}^S \end{bmatrix}^T$$

$$\Delta u_{Sc} = \begin{bmatrix} \Delta P_{ref} & \Delta Q_{ref} \end{bmatrix}^T$$

where, $\bar{V}_{d3}^S$ and $\bar{V}_{q3}^S$ represent the filtered values of the bus voltages, while $\bar{V}_{d3}^B$ and $\bar{V}_{q3}^B$ denote the filtered values of the converter voltages. Additionally, $\bar{i}_{d3}^S$ and $\bar{i}_{q3}^S$ represent the filtered values of the converter currents. The states of the PI controller for active and reactive power are denoted by Δi_{pd} and Δi_{qq}, respectively. Furthermore, ΔV_{pd} and ΔV_{qq} represent the PI controller states for the current control loops in the q and d axes, respectively.

2.4. State-Space Model of Network Including Feeders and Loads

Referring to the single-line diagram in Fig. 1, the dynamic model of the power network of the microgrid, in the stationary abc reference frame, can be expressed through ODEs for three-phase RL branches and parallel capacitors. These equations represent the relationships between buses current and voltage. The small-signal model of the power network, incorporating the DG units and framed in the d-q reference frame, can be outlined as follows:

$$\Delta\dot{x}_N = A_N\Delta x_N + B_N^{v1}\Delta v^W + B_N^{v2}\Delta v^D + B_N^{v3}\Delta v^S \qquad (17)$$

$$\Delta x_N = \begin{bmatrix} \Delta i_q^{L1} & \Delta i_d^{L1} & \Delta i_q^{L2} & \Delta i_d^{L2} & \Delta i_q^{L3} & \Delta i_d^{L3} & \Delta i_q^{L4} & \Delta i_d^{L4} & \Delta v_q^{PCC} & \Delta v_d^{PCC} \end{bmatrix}^T$$

Furthermore, the linearized equations governing the voltage vectors can be formulated as:

$$\Delta v^W = E_{11}^N\Delta x_N + E_{12}^N\Delta\dot{x}_N + D_{11}^N\Delta x_W + D_{12}^N\Delta\dot{x}_W$$

$$\Delta v^D = E_{21}^N\Delta x_N + E_{22}^N\Delta\dot{x}_N + D_{21}^N\Delta x_D + D_{22}^N\Delta\dot{x}_D \qquad (18)$$

$$\Delta v^S = E_{31}^N\Delta x_N + E_{32}^N\Delta\dot{x}_N + D_{31}^N\Delta x_S + D_{32}^N\Delta\dot{x}_S$$

2.5. Overall State-Space Model of the Microgrid System

The small-signal model for the microgrid system, incorporating multiple distributed generation sources, is derived by considering the individual models of DG1, DG2, BESS, and the power grid subsystems. Each subsystem is modeled based on its local reference frames. According to Figure 4, because the microgrid system comprises more than one DG unit, before developing the overall microgrid state-space model, all interfaced state variables of the subsystems should be transformed to a global reference frame, based on the transformation technique presented in (2). The input-output relationships governing these subsystems, including generation units, loads and power grid, are illustrated in the block diagram featured in Fig. 4. In this diagram, the output current components of the generation units serve as inputs to the power grid. Additionally, the output voltage vectors of the busbars in the power grid are considered as inputs into the dynamic model of the electric loads. The overall state-space model of the microgrid system, incorporating the detailed subsystem models outlined in equations 8, 12, 14, 16, and 17, is structured as follows:

$$\Delta\dot{x}_{MG} = A_{MG}\Delta x_{MG} + B_{MG}^u\Delta u_{MG} \qquad (19)$$

$$\Delta x_{MG} = \begin{bmatrix} \Delta x_W & \Delta x_D & \Delta x_{Sp} & \Delta x_{Sc} & \Delta x_N \end{bmatrix}^T$$

$$\Delta u_{MG} = \begin{bmatrix} \Delta u_W & \Delta u_D & \Delta u_S \end{bmatrix}^T$$

where Δx_{MG} and Δu_{MG} represent state vectors and the input signal vectors of microgrid consequently.
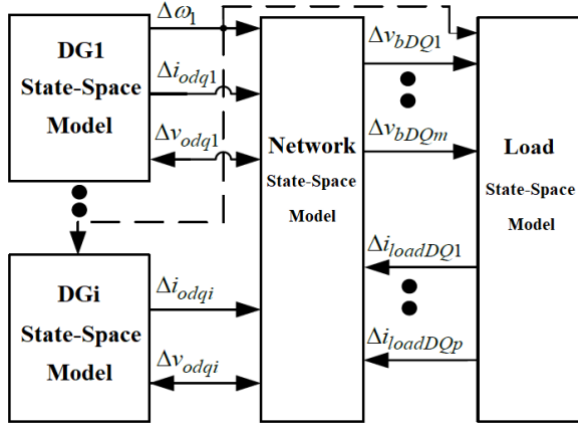

Fig. 4 block diagram of microgrid's small signal state-space model

3. Small Signal Stability Analysis of Microgrid

The linearized model of the microgrid system serves as a valuable tool for exploring the dynamic response of small signal within the microgrid and fine-tuning control parameters. This section employs the linearized model for two crucial analyses: (i) eigenvalue analysis and (ii) frequency response analysis, focusing on the transfer function of the BESS control system. The key parameters defining the microgrid system are detailed in Table 1. Furthermore, Fig. 5 and Table 2 show the positions and values of the eigenvalues, providing insight into the microgrid's behavior in a scenario where it operates independently from the main grid.

Table 1. System parameters

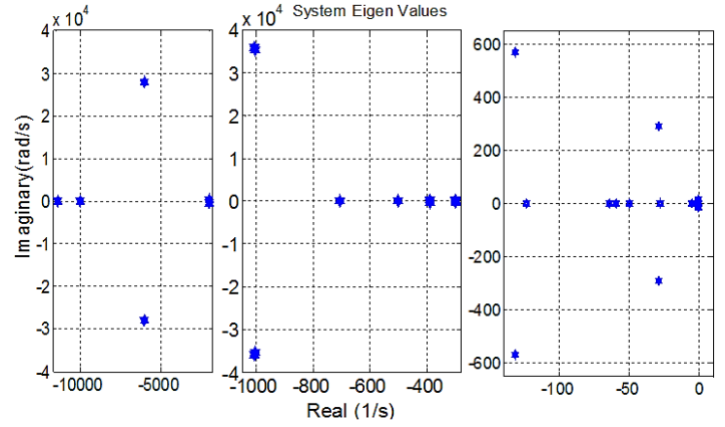| Element	Value
Voltage	400 V
Frequency	50 Hz
DG1	15 KVA
DG2	30 KVA
BESS	16 KVA
Line 1	0.0032+j0.005 Ω
Line 2	0.0032+j0.005 Ω
Line 3	0.0032+j0.005 Ω

Fig. 5. The placement of microgrid eigenvalues on the complex plane

Table 2. Eigenvalues of the autonomous microgrid

Eigen values	Real (1/s)	Im (rad/s)	Eigen values	Real (1/sec)	Im (rad/s)
1,2	-1004.95	±35910.97	25	-10000	0
3,4	-1004.19	±35282.67	26	-750.98	0
5,6	6016.23	±28003.58	27	-500	0
7,8	-131.08	±568.82	28	-289.11	0
9,10	-2012.87	±314.16	29	-129.39	0
11,12	-2010.62	±314.16	30	-63.84	0
13,14	-389.29	±314.16	31	-59.41	0
15,16	-28.45	±290.31	32	-50	0
17,18	-299.56	±282.05	33	-27.63	0
19,20	-0.5079	±14.96	34	-5.004	0
21	-11390.2	0	35	-2.47	0
22	-10000	0	36	-0.4047	0
23	-10000	0	37	-0.2498	0
24	-10000	0			

As indicated in Table 2, the microgrid exhibits 37 eigenvalues, all possessing negative real parts. Eigenvalues 1 to 20 form ten pairs of complex conjugate values, portraying the oscillatory modes within the system. As seen in Table 2 and Fig. 5, the low-frequency oscillatory modes are identified to be the dominant mode (with damping less than -400 s^{-1}), which is essential for the small signal stability analysis. Moreover, it can be seen that the dynamic characteristics of the proposed microgrid with multiple DG resources are noticeably affected by four pairs of eigenvalues, i.e., (7, 8), (13, 14), (15, 16) and (19, 20), which are also the dominant oscillatory modes. Specifically, eigen values (13,14) and (17,18) signify the active and reactive power support of DG2, illustrating electromagnetic reciprocal actions between DG2 and the equivalent grid. Similarly, eigen values (7,8) and (15,16) demonstrate the active and reactive power support of DG1, reflecting electromagnetic reciprocal actions between DG1 and the relevant grid.

4. Eigenvalues Analysis

The stability margin of the system under various operating conditions is determined by tracking the eigenvalues as changes occur in system parameters or operating states. To explore the dynamic stability margin of the microgrid and understand the sensitivity of eigenvalues to alterations in the operating point and control parameters, a sensitivity analysis method is employed.

The positions of eigenvalues (7, 8) and (15, 16) are visualized in Figs 6 and 7 as the capacity of DG1 (SCIG-WT) changes from 5 kVA to 25 kVA, maintaining constant wind speed conditions. The observation reveals a leftward movement of eigenvalues (7,8) with an increased DG1 capacity, signaling heightened mode damping and an improved stability margin in the system. In contrast, eigenvalue (15,16) shifts rightward, indicating reduced mode damping and a compromised stability region. Sensitivity analysis of DG1 under constant wind speed conditions highlights that augmenting its capacity results in an increased active power output and enhanced reactive power absorption. This suggests an improved capability to support active power, albeit with a weakened ability to support reactive power, thereby limiting the potential of renewable energy source installation.
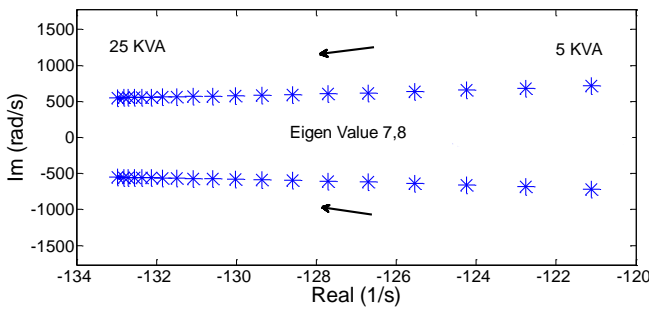

Fig. 6. Position of eigenvalues (7,8) with a change in DG1 capacity from 5 to 25 kVA
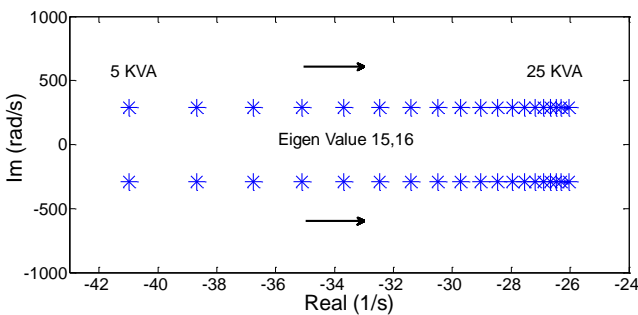

Fig. 7. Position of eigenvalues (15,16) with a change in DG1 capacity from 5 to 25 kVA

Sensitivity analysis has also been applied to explore the impact of microgrid poles when adjusting control parameters for the storage unit and electric load. This approach proves valuable in identifying the permissible range for these parameters. Parameters R_5 and X_5 indicate resistance and reactance of the load 2 respectively. In Fig. 8 and 9, an increase in R_5 results in eigenvalues 19 and 20 entering the right half of the imaginary axis, pushing the microgrid into an unstable region. Additionally, an escalation in reactance X_5 causes eigenvalues 19 and 20 to shift leftward, transitioning from oscillatory behavior to two real eigenvalues moving in opposite directions.
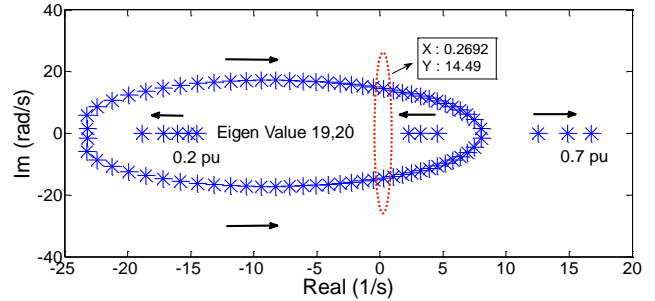

Fig. 8. The position of eigenvalues (19,20) with changes in the resistance R_5 from 0.2 to 0.7
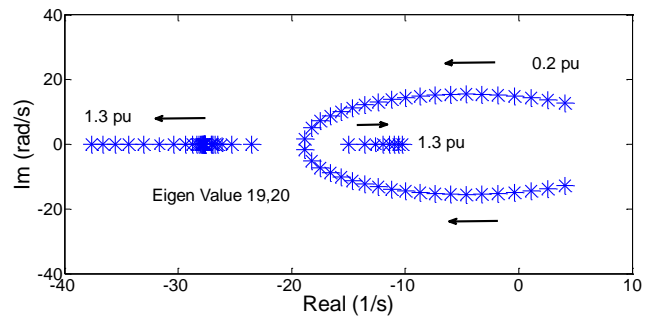

Fig. 9. The position of eigenvalues (19,20) with changes in reactance X_5 from 0.2 to 1.3

5. Frequency Response Analysis

The provided linear model given by 19 is utilized to derive transfer functions between input and output signals corresponding to active $\left(\frac{\Delta i_d^S}{\Delta P_{out}}\right)$ and reactive power $\left(\frac{\Delta i_q^S}{\Delta Q_{out}}\right)$ controllers of the BESS. The transfer functions equations present at appendix.

In order to investigate the effect of each parameter of the BESS active and reactive power controllers on the frequency response, each parameter is changed, and magnitude and phase angle of the transfer function associated with active and reactive power controllers are plotted. These diagrams help to study the resonant frequency and system sensitivity to changes in each parameter. Additionally, they can be utilized to determine the gain and phase margins, representing the impact of parameter variations on these margins. Overlaying a shaded region on these diagrams can assist in determining the worst-case gain and phase margins, ensuring system stability.

The impact of real power controller parameters T_i, K_{pd}, and K_{pi} on the frequency response of the transfer function $\frac{\Delta i_d^S}{\Delta P_{out}}$ is showcased in Figs 10 to 12. In Fig. 10, variations in T_i exhibit a noticeable effect on mid-range frequencies, with the resonant frequency decreasing as T_i increases. Conversely, Fig. 11 highlights the substantial impact of K_{pd} on high frequencies, with its increase maintaining a constant resonant frequency. Figure 12 further demonstrates the impact of K_{pi} on mid-range frequencies, where an increase in K_{pi} leads to a resonant frequency rise.
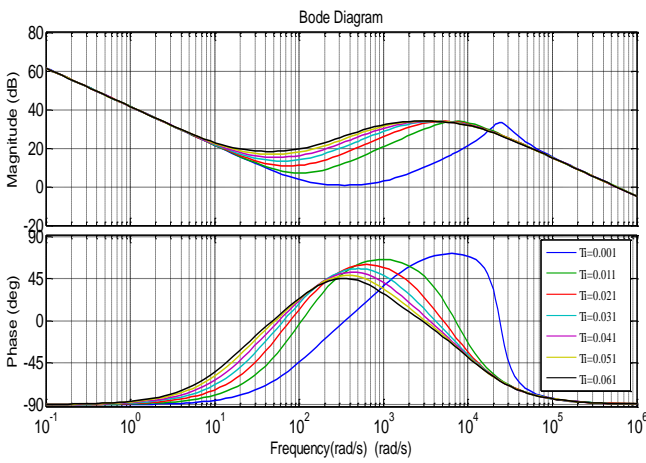
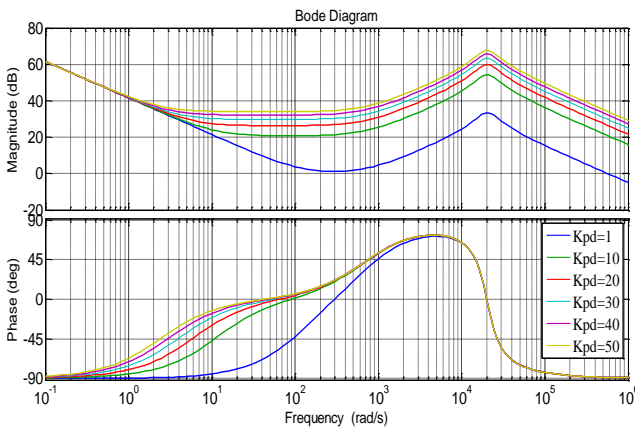**Fig. 10.** Sensitivity of the $\frac{\Delta i_d^S}{\Delta P_{out}}$ to changes in T_i

Fig. 11. Sensitivity of the $\frac{\Delta i_d^S}{\Delta P_{out}}$ to changes in K_{pd}
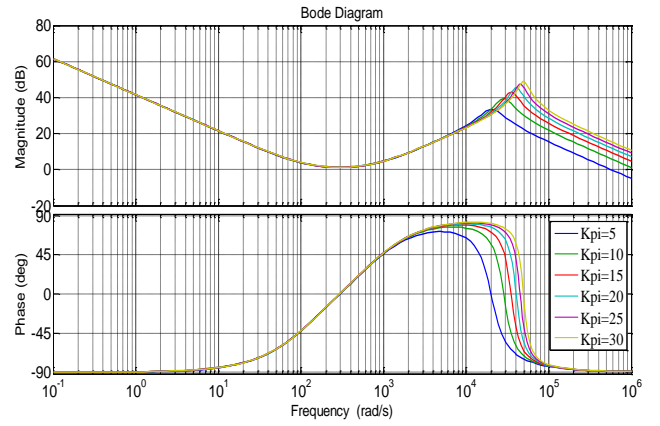

Fig. 12. Sensitivity of the $\frac{\Delta i_d^S}{\Delta P_{out}}$ to changes in K_{pi}

Furthermore, the impact of reactive power controller parameters T_i, K_p, and K_{pv} on the frequency response of the transfer function is illustrated in Figs 13 to 15. From Figure 13, it can be observed that the system's sensitivity to changes in T_i is negligible at mid-range frequencies. However, Fig. 14 and 15 indicate that increasing K_{pv} and K_p affect the system's behavior at higher frequencies, while the magnitude of the resonant frequency remains nearly constant.
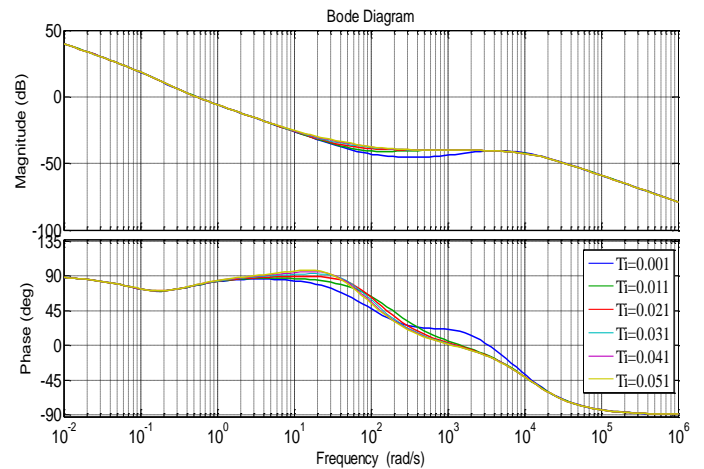

Fig. 13. Sensitivity of the $\frac{\Delta i_d^S}{\Delta Q_{out}}$ to changes in T_i
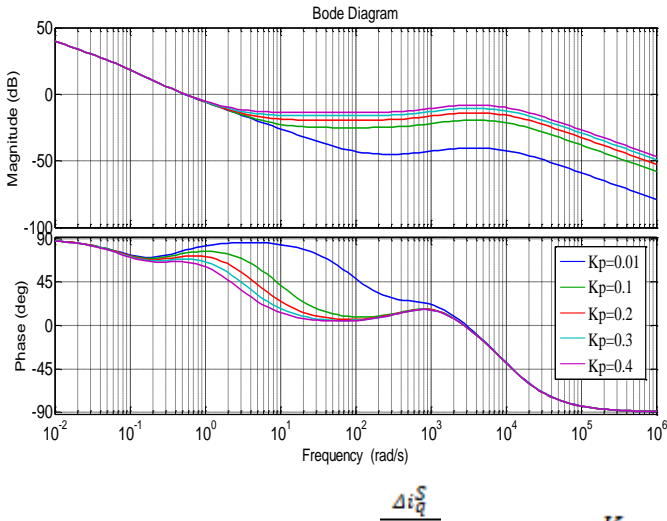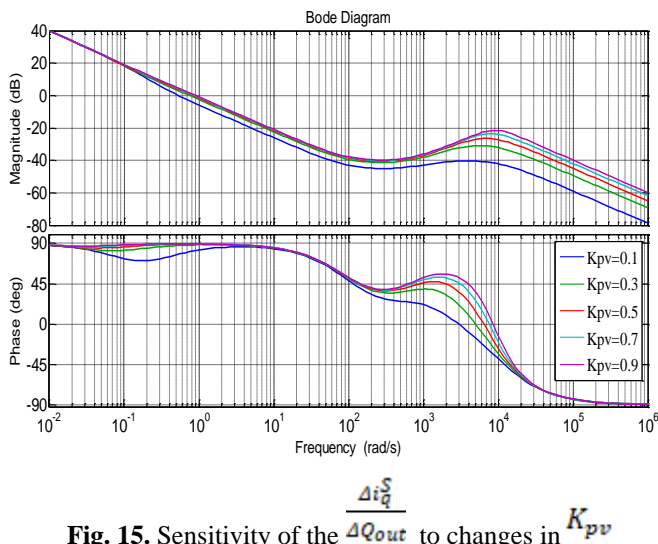
Fig. 14. Sensitivity of the $\dfrac{\Delta i_q^S}{\Delta Q_{out}}$ to changes in K_p

Fig. 15. Sensitivity of the $\dfrac{\Delta i_q^S}{\Delta Q_{out}}$ to changes in K_{pv}

6. Conclusion

This research presents the dynamic model of an independent microgrid within a rotating reference frame tailored for studying small-signal dynamics, incorporating the models of each DG source. The diverse DG sources, including a wind turbine with an induction generator, a synchronous diesel generator, and a battery energy storage unit with a converter and controller, were initially individually modeled in their local state spaces. Subsequently, these models were amalgamated in a global reference frame. This approach offers versatility for developing small-signal dynamic models for various microgrids featuring different numbers of DG sources. The examination of the microgrid's dynamics involved assessing the influence of altering system parameters and diverse operating conditions. Based on the state-space model, displacement of eigenvalues analysis was carried out to reveal dynamic stability margin of the LV microgrid and identify the permissible variations range of the DG capacity,

load and control parameters. The findings reveal that the dynamic stability of microgrids is intricately linked to factors such as the system configuration, dominant modes related to electromagnetic interactions of DG units such as (7, 8), (13, 14), (15, 16), and the chosen control strategy. Moreover, the study delved into the impact of controller coefficients on the frequency response of transfer functions corresponding to the active and reactive power controller for BESS. By analyzing changes in each coefficient and plotting Bode diagrams, the study scrutinized frequency shifts (resonant frequency) and system sensitivity to variations in each coefficient. The frequency responses have provided comprehensive information on the dominant modes in the controllers, i.e. at frequencies 10, 10000 and 20000 rad/s. The bode plots can be utilized to provide a satisfactory compromise between the bandwidth of input‚output transfer functions to achieve reference tracking at all input frequencies, and to maintain stability of the control loops during transients. The linearized model also can be used to develop open-loop transfer function of the system to determine the stability margin and design the controllers of BESS. Considering photovoltaic system and dynamic load model in stability analysis of microgrid are some recommendations in future studies. Selection of induction motor loads can be satisfying in an advanced analysis aiming to provide a more exact view on the microgrid stability.

References

[1] M. M. Sayed, M. Y. Mahdy, S. H. Abdel Aleem, H. K. Youssef, T. A. Boghdady, "Simultaneous Distribution Network Reconfiguration and Optimal Allocation of Renewable-Based Distributed Generators and Shunt Capacitors under Uncertain Conditions. Energies, Vol. 15, No. 6, pp. 2299, 2022.

[2] S. Choudhury, "A comprehensive review on issues, investigations, control and protection trends, technical challenges and future directions for Microgrid technology". International Transactions on Electrical Energy Systems . Vol. 30, No. 9, pp. 12446, 2020.

[3] A. Mohammed, S. S. Refaat, S. Bayhan, H. Abu-Rub, "Ac microgrid control and management strategies: Evaluation and review". IEEE Power Electronics Magazine, Vol. 6, No. 2, pp. 18–31, 2019.

[4] R. Majumder, "Some aspects of stability in microgrids" IEEE Transactions on power systems, Vol. 28, pp. 3243-3252, 2013.

[5] Z. Shuai, Y. Sun, Z. J. Shen, W. Tian, C. Tu, Y. Li, X. Yin, "Microgrid stability: Classification and a review". Renewable and Sustainable Energy Reviews. Vol. 58, pp. 167-179, 2016.

[6] S. Wang, J. Su, X. Yang, Y. Du, Y. Tu, H. Xu, "A review on the small signal stability of microgrid," IEEE 8th International Power Electronics and Motion Control Conference (IPEMC-ECCE Asia), Hefei, China, 2016, pp. 1793-1798, May 2016.

[7] E. A. Mohamed, G, Magdy, G. Shabib, A. A. Elbaset, Y. Mitani, "Digital coordination strategy of protection and frequency stability for an islanded microgrid". Transmission Distribution IET Generation Vol. 12, No. 15, pp. 3637–3646. 2018.

[8] Y. Yan, D. Shi, D. Bian, B. Huang, Z. Yi and Z. Wang, "Small-Signal Stability Analysis and Performance Evaluation of Microgrids Under Distributed Control," IEEE Transactions on Smart Grid, Vol. 10, No. 5, pp. 4848-4858, Sep. 2019.

[9] S. Leitner, M. Yazdanian, A. Mehrizi-Sani, A. Muetze, "Small-signal Stability Analysis of an Inverter-based Microgrid with Internal Model–based Controllers", IEEE Transactions on Smart Grid, Vol. 9, No. 5, pp. 5393-5402, 2017.

[10] R. Agrawal, D. D. Changan, A. Bodhe,."Small signal stability analysis of stand-alone microgrid with composite load", Journal of Electrical Systems and Information Technology, Vol. 7, No. 1, pp. 12, 2020.

[11] A. Mahdavian, A. A. Ghadimi, M. Bayat, "Microgrid small-signal stability analysis considering dynamic load model". IET Renewable Power Generation, Vol. 15, No. 13, pp. 2799-2813, 2021.

[12] S. M. Malik, Y. Sun, X. Ai, Z. Chen, K. Wang, "Small-signal analysis of a hybrid microgrid with high PV penetration". IEEE access, Vol. 7, pp. 119631-119643, 2019.

[13] D. K. Dheer, N. Soni, S. Doolla, "Improvement of small signal stability margin and transient response in inverter-dominated microgrids". Sustainable Energy, Grids and Networks, Vol. 5, pp. 135-147, 2016.

[14] Y. Levron, J. Belikov, "Modeling power networks using dynamic phasors in the dq0 reference frame. Electric Power Systems Research, Vol. 144, pp. 233-242, 2017.

[15] D. K. Dheer, S. Doolla, S. Bandyopadhyay, J. M. Guerrero, "Effect of placement of droop-based generators in distribution network on small signal stability margin and network loss". International Journal of Electrical Power & Energy Systems, Vol. 88, pp. 108-118, 2022.

[16] J. Schiffer, D. Zonetti, R. Ortega, A. M. Stanković, T. Sezi, J. Raisch, "A survey on modeling of microgrids—From fundamental physics to phasors and voltage sources. Automatica. Vol. 74, pp. 135-150, 2016.

[17] H. Liang, B. J. Choi, W. Zhuang, X. Shen, "Stability enhancement of decentralized inverter control through wireless communications in microgrids", IEEE Trans. Smart Grid, Vol. 4, no. 1, pp. 321-331, 2013.

[18] K. Yamashita, H. Renner, et al, Modelling of inverter-based generation for power system dynamic studies, CIGRE, 2018.

[19] F. Katiraei, M. R. Iravani, P. W. Lehn, "Small-signal dynamic model of a microgrid including conventional and electronically interfaced distributed resources", IET generation, transmission & distribution, Vol. 1, No. 3, pp. 369–378, 2007.

[20] T. Ma, X. Jin, X. Huang, "Modeling and Stability Analysis of Microgrid with Multiple Converters", Automation of Electric Power Systems, Vol. 37, No. 6, pp. 12–17, Mar. 2013.

[21] J. A. Mueller, J. W. Kimball, "Reduced-Order Small-Signal Model of Microgrid Systems", IEEE Trans. Sustain. Energy, Vol. 6, No. 4, pp. 1292–1305, 2015.

[22] P. C. Krause, O. Wasynczuk, S. D. Sudhoff, S. Pekarek, "Analysis of electric machinery and drive systems", Vol. 2. New York: IEEE press. 2002.

[23] A. G. Tsikalakis, N. D. Hatziargyriou, "Centralized control for optimizing microgrids operation", in 2011 IEEE power and energy society general meeting, pp. 1-8, 2011.

Appendix

The transfer functions corresponding to the active power $\left(\frac{\Delta i_d^S}{\Delta P_{out}}\right)$, reactive power $\left(\frac{\Delta i_q^S}{\Delta Q_{out}}\right)$, of the BESS controller:

$$G_1(s) = \frac{\Delta i_d^S}{\Delta P_{out}} = \frac{0.007 s^3 + 5.875 s^2 + 629.2 s + 3000}{1.23 * 10^{-8} s^4 + 0.0001488 s^3 + 5.1 s^2 + 25 s}$$

$$G_2(s) = \frac{\Delta i_q^S}{\Delta Q_{out}} = \frac{1.4 * 10^{-6} s^3 + 0.0009668 s^2 - 0.02376 s - 0.006}{1.23 * 10^{-8} s^4 + 0.0001488 s^3 + 0.2 s^2 + 0.025 s}$$